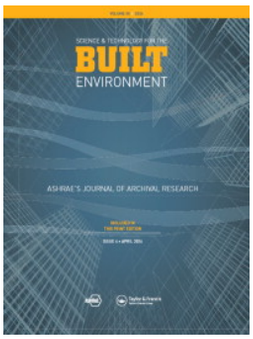

Taylor & Francis
Taylor & Francis Group

Science and Technology for the Built Environment

ISSN: (Print) (Online) Journal homepage: www.tandfonline.com/journals/uhvc21

Multi-scenario Extreme Weather Simulator application to heat waves: Ko'olauloa community resilience hub

Daniel L. Villa, Sang Hoon Lee, Carlo Bianchi, Juan Pablo Carvallo, Illya Azaroff, Andrea Mammoli & Tyler Schostek

To cite this article: Daniel L. Villa, Sang Hoon Lee, Carlo Bianchi, Juan Pablo Carvallo, Illya Azaroff, Andrea Mammoli & Tyler Schostek (2024) Multi-scenario Extreme Weather Simulator application to heat waves: Ko'olauloa community resilience hub, Science and Technology for the Built Environment, 30:4, 375-393, DOI: 10.1080/23744731.2023.2279467

To link to this article: https://doi.org/10.1080/23744731.2023.2279467

Published online: 20 Dec 2023.

Science and Technology for the Built Environment, (2024) **30**, 375–393

ISSN: 2374-4731 print / 2374-474X online
DOI: 10.1080/23744731.2023.2279467

Multi-scenario Extreme Weather Simulator application to heat waves: Ko'olauloa community resilience hub

DANIEL L. VILLA[1]*, SANG HOON LEE[2], CARLO BIANCHI[3], JUAN PABLO CARVALLO[2], ILLYA AZAROFF[4], ANDREA MAMMOLI[1] and TYLER SCHOSTEK[5]

[1]*Sandia National Laboratories, Albuquerque, NM, USA*
[2]*Lawrence Berkeley National Laboratory, Berkeley, CA, USA*
[3]*National Renewable Energy Laboratory, Boulder, CO, USA*
[4]*+Lab Architect PLLC, Brooklyn, NY, USA*
[5]*Purdue University, West Lafayette, IN, USA*

Heat waves are increasing in severity, duration, and frequency. The Multi-Scenario Extreme Weather Simulator (MEWS) models this using historical data, climate model outputs, and heat wave multipliers. In this study, MEWS is applied for planning of a community resilience hub in Hau'ula, Hawaii. The hub will have normal operations and resilience operations modes. Both these modes were modeled using EnergyPlus. The resilience operations mode includes cutting off air conditioning for many spaces to decrease power requirements during emergencies. Results were simulated for 300 future weather files generated by MEWS for 2020, 2040, 2060, and 2080. Shared socioeconomic pathways 2–4.5, 3–7.0 and 5–8.5 were used. The resilience operations mode results show two to six times increase of hours of exceedance beyond 32.2 °C from present conditions, depending on climate scenario and future year. The resulting decrease in thermal resilience enables an average decrease of energy use intensity of 26% with little sensitivity to climate change. The decreased thermal resilience predicted in the future is undesirable, but was not severe enough to require a more energy-intensive resilience mode. Instead, planning is needed to assure vulnerable individuals are given prioritized access to air-conditioned parts of the hub if worst-case heat waves occur.

Introduction

Paleoclimate data, meteorological measurements, and global circulation model results reveal unequivocally that Earth's climate is changing at unprecedented rates compared to the last millennia (Hausfather 2018). Among other weather anomalies, climate change is increasing the frequency, duration, and intensity (FDI) of heat waves (HWs) (Keellings and Moradkhani 2020; Bekris, Loikith, and Neelin 2023). World Weather Attribution (WWA) found that HWs in southern Europe, the United States, and Mexico in summer 2023 were "virtually impossible" without anthropogenic warming (WWA 2023). Such extreme temperatures severely stress critical infrastructure and jointly affect mutually dependent systems such as the electric grid, gas pipelines, and buildings (White et al. 2023; Lee, Maron, and Mostafavi 2022). As a result, immediate action is needed to mitigate greenhouse gases (GHG) emissions and to assure infrastructure can adequately survive and protect humanity from increased FDI of HWs.

Mitigation and adaptation through buildings

Buildings play an important role in mitigating GHG emissions because they are responsible for almost 40% of energy- and process-related GHG emissions globally (IEA 2019). If electric loads are reduced and managed in optimal ways within buildings, less grid infrastructure and electricity-producing resources are needed to support a larger load across the electric grid (Munankarmi et al. 2021). Also, significant benefits can result for building owners (Lokeshgupta and Ravivarma 2023). Hence, many efforts have focused on increasing the energy efficiency of

Received June 7, 2023; accepted October 16, 2023
Daniel L. Villa, MME, PE, Full Member ASHRAE, is a Principal Member of Technical Staff. **Sang Hoon Lee, PhD,** is a Senior Scientific Engineering Associate. **Carlo Bianchi, PhD, Associate Member ASHRAE,** is a Commercial Buildings Research Group Staff Member. **Juan Pablo Carvallo, PhD,** is a Research Scientist. **Illya Azaroff, FAIA,** is the Founding Principal of +Lab Architect PLLC. **Andrea Mammoli, PhD,** is a Principal Member of Technical Staff. **Tyler Schostek, MS,** is a PhD Student.
*Corresponding author e-mail: dlvilla@sandia.gov

buildings to produce an energy transition to a carbon-neutral world (Cabeza and Chafer 2020; De la Pena et al. 2022).

Buildings also have an important role in climate change adaptation—especially for their performance under increased FDI of HWs. Much of the global population relies on air conditioning (A/C) and refrigeration for survival during extreme heat. The likelihood of these systems failing under the high stress of extreme temperature events depends on availability of electricity. Power failures can therefore lead to sickness and mortality during extreme heat (Sun, Specian, and Hong 2020). Design of building performance during power outages is therefore critical. Striking a balance between competing needs for thermal resilience during power outages and minimization of cost for normal conditions is not easy. To be comprehensive, a Monte Carlo-type study is needed to understand the relationship between extreme outcomes (e.g., loss of life in a building due to future HWs) and normal design issues (e.g., energy efficiency, sustainable design, etc.).

Building energy modeling

A building energy model (BEM) can be based on statistical analysis of energy data (i.e., data-driven), physics-based, or hybrids of data-driven and physic-based approaches (Chen et al. 2022). For applications that require years of simulation time into the future, physics-based modeling is the most effective approach. Physics-based BEMs are inputs to software that solve the convective, conductive, and radiative heat balance equations over time. Ambient conditions outside a building provide boundary conditions to these equations. Significant simplifications to three-dimensional space–time are needed to make simulation of a building's thermal systems practical. As a result, one-dimensional networks that connect at nodes in three-dimensional space are used. Thermal and mass balances are computed at these nodes with simplification for how fluid mixing and radiation scattering and absorption occur.

Building energy simulation (BES) tools such as the U.S. Department of Energy's EnergyPlus software (DOE 2023a) and DOE-2 (Hirsch and Associates 2023) can be used by modelers to create BEMs through text inputs. Many software packages leverage these and other BES tools to create graphical user interfaces for constructing BEMs efficiently. For this study, the OpenStudio software, which leverages EnergyPlus, was used to construct a set of BEMs (DOE 2023b; Brackney et al. 2018).

Multi-scenario Extreme Weather Simulator

Building energy modelers face a tremendous challenge to include the effects of extreme events in their models. This has motivated development of the Multi-scenario Extreme Weather Simulator (MEWS). MEWS enables studies of the effects future HWs will have on buildings (Villa et al. 2023). MEWS operates in two stages. First, it reads 50 or more years of National Oceanic and Atmospheric Administration (NOAA) daily summary data to characterize the FDI of historic HWs and cold snaps (CSs). Second, it increases the FDI of HWs based on mean surface temperature increase from 2014 by shifting and stretching the historic HW distributions according to factors obtained from the Intergovernmental Panel on Climate Change (IPCC). Though CSs are naturally included in the MEWS algorithms, this study does not shift CS statistics due to insufficient scientific consensus on how CSs will change in the future (Cohen et al. 2020). More recent studies have shown an increase in severity of CSs, but information usable by MEWS is not yet developed (Hong et al. 2023). This study therefore assumes CSs are unaltered.

The results from MEWS are shifted statistical distributions of HWs' peak temperature and duration. These shifted distributions can be used in building energy modeling to produce well-informed risk assessments. The results can be used for scenario-based resilience analysis or for stochastic methods. For a scenario-based approach, the HWs distribution is integrated to a desired level of risk such as a 1 in 50-year HW. The resulting HW magnitude can then be added to a single year of downscaled future conditions to analyze worst-case heat conditions for a future year. Several different risk levels could also be assessed for a single study this way if a range of outcomes is desired. The stochastic approach requires much more computation but enables full characterization of infrastructure systems responses for the entire range of expected future heat outcomes. MEWS is implemented to produce thousands of stochastic HW and CS patterns that can be applied using Monte Carlo approaches to simulations of infrastructure systems. MEWS is set up to produce weather files that can be used by both EnergyPlus and DOE-2.

Ko'olauloa Community Resilience Hub

In this study, a new community resilience hub being designed in Hau'ula, HI, is analyzed using MEWS weather files. Primarily serving as a community center, the Ko'olauloa Community Resilience Hub (KCRH) is designed to "near absolute protection" using Federal Emergency Management Agency (FEMA) P-320 and P-361 guidance (FEMA 2021a, 2021b). The need for the KCRH is driven by a history of isolation after extreme weather events in Hau'ula. The KCRH therefore must be designed with two operational modes: (1) normal operations (NormOps), where the center serves to provide a vibrant atmosphere for community events, and (2) resilience operations (ResOps), where space use, HVAC, and electric power are configured to minimize danger and discomfort to the surrounding communities after a disaster that has isolated Hau'ula.

The Hau'ula community can only be accessed via the Kamehameha Highway (Highway 83), which often becomes impassable after extreme weather events. Communities in the area can be isolated for up to 30 days with no grid power after an extreme weather event. The current local community center becomes a hub of resilience services under such conditions. In major extreme events such as hurricanes, thousands of people in the surrounding communities can become isolated. Emergency preparedness therefore makes it desirable to build a larger community center that serves as a storm shelter and resilience hub to the surrounding communities during both normal and emergency conditions. This center must be designed to handle prolonged resilience scenarios including a strike from a powerful hurricane. The KCRH is designed to maintain operation in the event of a

major hurricane where electricity, water, and lifeline medical services may be compromised. It therefore will employ a microgrid to assure services to the surrounding community. The climate-aware community also desires to make the design highly efficient and sustainable.

Research questions

This study uses MEWS and BEMs to address the following research questions: (1) How much difference will stochastic future extreme temperature events for 2040, 2060, and 2080 in Hau'ula affect energy loads and thermal resilience of both the NormOps and ResOps of the KCRH? (2) Will occupant thermal comfort issues become unacceptably high for ResOps in the KCRH in the future? To answer these questions, we conduct a MEWS analysis with weather information from Kane'ohe Bay, the closest coastal weather station from which Typical Meteorological Year (TMY) data are available. We take the Kane'ohe Bay hourly data and adjust them using monthly climate variables to create a morphed weather file that is more representative of Hau'ula for dry bulb temperature, solar radiation, and ground temperatures. We also create two BEMs of the KCRH for NormOps and ResOps.

This article commences with a brief literature review of stochastic weather generation and BEM climate change studies. It then provides the methods and procedure to quantify HWs with a subsequent description of the BEM study. The results are then presented for the specified metrics. followed by conclusions of the study.

Literature review

Since this study uses MEWS and BEMs, the literature review focuses on (1) existing models to produce synthetic weather data and (2) impact of climate-change-induced HWs on buildings.

Calibrated regional climate models such as the Coordinated Climate Downscaling Experiments (CORDEX) (CORDEX 2021; Sylla et al. 2011; Meehl et al. 2018; Grossman-Clarke et al. 2014) have progressed enough to make global estimations of increases in FDI of extreme weather events. Multiple recent studies have proposed statistical models to capture the FDI of HWs due to climate change (Cowan et al. 2014; Ragone, Wouters, and Bouchet 2018; Abadie, Chiabai, and Neumann 2019). Methods to produce stochastic synthetic weather data have been proposed to (1) project current weather data, accounting for climate change effects (Rastogi and Andersen 2016; Rastogi and Khan 2021; Semenov and Barrow 2002), (2) run sensitivity analyses on BEM in the absence of complete historical weather data for a given location (Aguiar, Camelo, and Goncalves 1999; Rastogi, Khan, and Andersen 2022), (3) simulate extreme weather conditions respecting the realistic weather patterns of the considered location (Adelard et al. 2012), and (4) model typical weather conditions (Rastogi and Andersen 2015; Bass, New, and Wade 2022). Farah, Saman, and Boland (2018) proposed a method to produce robust stochastic weather data using only typical data, without needing historical weather data. However, only a few of these methods and models are intended to be used directly for building performance simulation, including the need to produce consistent weather inputs for BEMs. Further review of this topic is available in the literature (Zeng et al. 2023).

Multiple studies in the literature have confirmed how historic typical weather data fail to capture the effects of a changing climate on buildings (Siu and Liao 2020; Yassaghi, Mostafavi, and Hoque 2019). Studies concerning buildings and climate change have focused on (1) how energy retrofits are affected by climate change (De Masi et al. 2021; Akkose, Akgul, and Dino 2021; Hosseini, Tardy, and Lee 2018), (2) clear trends in increased energy demand using current weather data compared to typical meteorological data based on the last couple of decades (Koci et al. 2019; Hosseini, Tardy, and Lee 2018; Bianchi and Smith 2019), (3) energy use intensity (EUI), heating, and cooling demand changes in entire regions (Yang, Javanroodi, and Nik 2021; Fonseca, Nevat, and Peters 2020), (4) future typical meteorological conditions (Bass and New 2023), and (5) how net-zero energy buildings will perform in the future (D'Agostino et al. 2022).

Power outages due to HWs are also an important aspect of analysis of future resilience. A good review of resilience metrics in terms of HWs and power outages in the built environment is provided by Attia et al. (2021). Studies of resilience measures with regard to extreme heat or cold include loss of productivity due to power outages correlated to extreme heat conditions (Mathew et al. 2021), thermal comfort and survivability (Sun, Specian, and Hong 2020; Rahif, Amaripadath, and Attia 2021), and changes in peak load and energy consumption (Villa 2021). Resilient cooling strategies critical for buildings to provide resistance, robustness, and recoverability during power outages are explored by Zhang et al. (2021). Zhang et al. (2021) also provide a critical review of resilience measures to mitigate high indoor air temperature during HWs. ASHRAE 55-2017 provides the standard effective temperature metric to evaluate human response to heat stress during HWs (ASHRAE 2017; Zhang et al. 2023).

Our search of the literature indicates that application of MEWS for Monte Carlo studies applied to BEM analyses has been mostly addressed by our own work. This study is unique because it enables trade-offs that fully develop joint distributions between energy efficiency and thermal comfort for future HW conditions.

This study is an extension to resilience analysis of the original SimBuild conference paper on MEWS (Villa et al. 2022). A more extensive review of MEWS and of stochastic weather generation techniques is provided in our recent publication (Villa et al. 2023). Since the SimBuild paper, MEWS has undergone significant updates. It was found that accuracy using algebraic methods could not be achieved past 2060. The assumption that variables were uncorrelated no longer held. As a result, an optimization technique is used. Also, the Sixth Coupled Model Intercomparison Project (CMIP6) data are automatically used by MEWS, making analysis at any NOAA station with daily summaries for

more than 50 years and climate normals feasible. This also makes application of various shared socioeconomic pathway (SSP) scenarios straightforward.

Methods

Methods for MEWS are first discussed, followed by a description of the case study and BEMs used.

MEWS overview

For extreme temperature events in MEWS, a minimal complexity process was sought that (1) characterizes the historical statistics and (2) can extrapolate increasing FDI as defined by the IPCC. Figure 1 shows the steps used by MEWS.

Starting with NOAA climate normals (NOAA 2021b) and daily summaries (NOAA 2021a), FDI histograms for CSs and HWs are calculated. The initial values for optimizing the MEWS stochastic model described in Villa et al. (2023, section 2.1) are then calculated. Previously, these values were the final values for a MEWS analysis such as in the first MEWS study (Villa et al. 2022). The results were inadequate for projections past 2060, though. This led to the development of the third step that involves use of a genetic algorithm to optimize 14 parameters of the MEWS model for each month. A postprocessing step after this involves calculation of the Kolmogorov–Smirnov test statistics to evaluate whether the historic histograms match the MEWS model with 95% confidence. Step 5 entails fitting polynomials to CMIP6 surface temperatures so that increases in FDI can be estimated using IPCC increase factors shown in Table 1. The rest of the steps moving upward are then repeatedly applied using the stochastic model for different years, scenarios, and confidence intervals on FDI factors from Table 1. Step 6 sets thresholds for 10- and 50-year events for future years by shifting the historic 10- and 50-year events using the polynomials from step 5 and IPCC factors. These thresholds are then used in step 7 to produce new MEWS model distributions that have least-squares optimal fit thresholds to the shifted historic thresholds. These new distributions then either can be used directly to assess worst-case peak temperature for constructing a resilience scenario or can be sampled to form synthetic HW and CS histories that can be added to TMY temperatures.

MEWS model

MEWS uses a three-by-three right-handed state transition stochastic matrix M_m for each month m. The first row represents nonextreme temperatures and includes the probability of entering a CS in month m in the next time step, $P_{cs,m}$, and the probability of entering an HW in the next time step, $P_{hw,m}$. These are the first two of 14 total parameters that are optimized to fit historical HW and CS distributions.

$$M_m(\Delta t) = \begin{bmatrix} 1 - P_{hw,m} - P_{cs,m} & P_{cs,m} & P_{hw,m} \\ 1 - P_{s_{cs,m}}(\Delta t) & P_{s_{cs,m}}(\Delta t) & 0 \\ 1 - P_{s_{hw,m}}(\Delta t) & 0 & P_{s_{hw,m}}(\Delta t) \end{bmatrix} \tag{1}$$

Here, Δt is the total time steps since a CS or HW began. The second row contains probabilities of sustaining a CS, $P_{s_{cs,m}}(\Delta t)$, in the next time step after Δt time steps. The third row contains the probability of sustaining HWs, $P_{s_{hw,m}}(\Delta t)$. Rather than being constant like the first row, the P_s terms are functions of the following form where w is the event index ($w = \{cs, hw\}$):

$$P_{s_{w,m}}(\Delta t) = \begin{cases} P_{0_{w,m}}\left(1 + \left(\frac{\Delta t}{\Delta t_{p_{w,m}}}\right)^2 e^2 \left(\frac{P_{max_{w,m}}}{P_{0_{w,m}}} - 1\right) e^{-2\frac{\Delta t}{\Delta t_{p_{w,m}}}}\right) & \Delta t \le 2\Delta t_{p_{w,m}} \\ P_{0_{w,m}} e^{-e^{-2\left(\frac{\Delta t}{\Delta t_{p_{w,m}}} - 2\right)^2 \left|\frac{P_{max_{w,m}}}{P_{0_{w,m}}} - 1\right|}} & \Delta t \le \Delta t_{c_{w,m}} \\ \left(1 + \left(\frac{\Delta t}{\Delta t_{p_{w,m}}}\right)^2 e^2 \left(\frac{P_{max_{w,m}}}{P_{0_{w,m}}} - 1\right) e^{-2\frac{\Delta t}{\Delta t_{p_{w,m}}}}\right) & \\ 0.0 & \Delta t > \Delta t_{c_{w,m}} \end{cases} \tag{2}$$

This functional form gives eight more parameters (four for CSs and four for HWs) out of the 14 model parameters. $P_{0_{w,m}}$ is the initial probability of sustaining a wave, $\Delta t_{p_{w,m}}$ is the time to peak probability $P_{max_{w,m}}$, and $\Delta t_{c_{w,m}}$ is a cutoff time at which probability is immediately reduced to zero. Figure 2 shows a nondimensional view of this function's form for three ratios of $P_{\max}/P_0$. The use of this function was found to be critical to enable realistic characterization of HW and CS dynamics. The capacity for probability to increase, decrease, and then cut off greatly improved fits to HW and CS distributions. A constant probability tends to enable too many overly short and long events. The functional form of Equation 2 enables centering on actual durations more accurately.

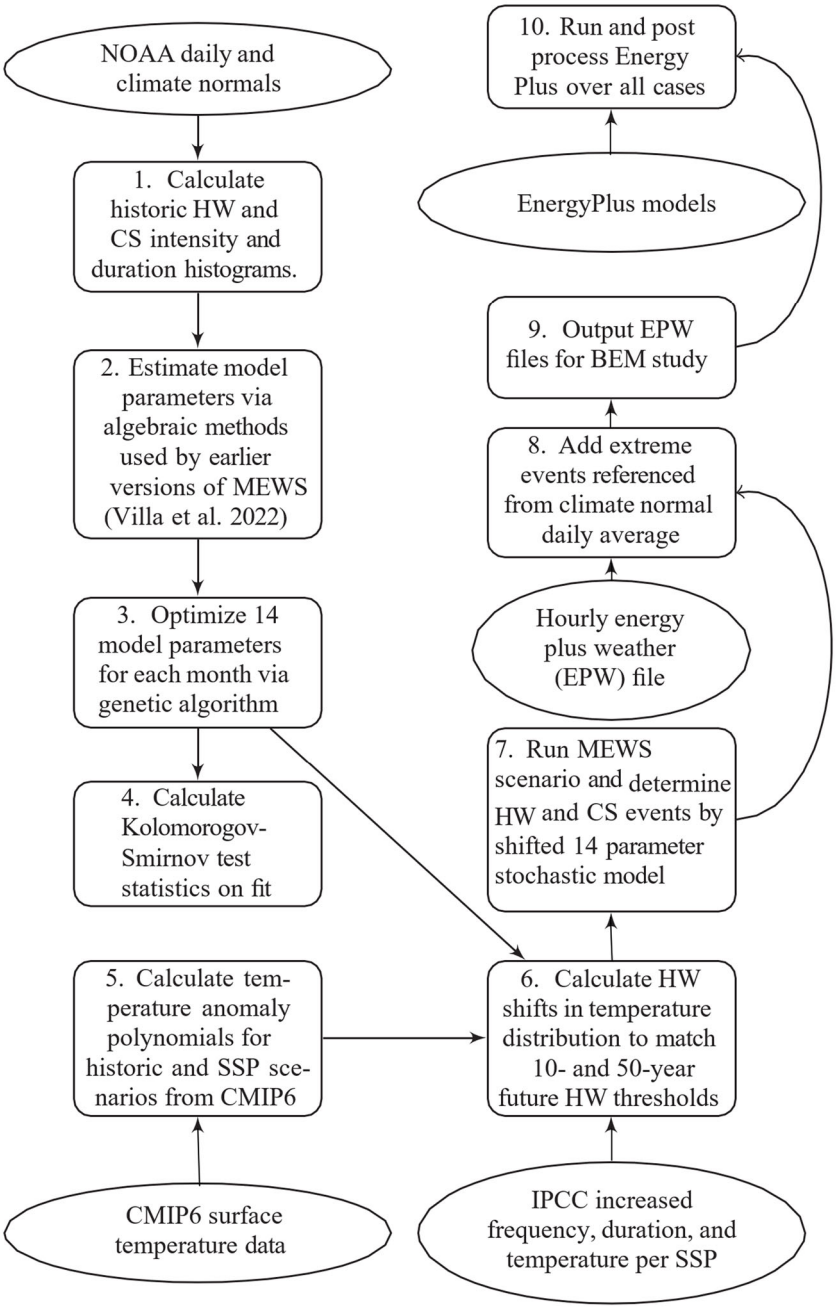

Fig. 1. Overview of MEWS and BEM study process. Ovals portray analysis inputs and boxes indicate steps. The left-hand-side process is only executed once for historical fits, while the right-hand-side process is executed over SSP scenario, future year, HW FDI confidence interval, BEM model, and realization number.

The transition matrix shown in Equation 1 defines the duration of events. The severity of events is correlated to the duration but also contains a random sampling of both total energy of an HW and peak temperature. In MEWS, a linear regression of duration versus extreme temperature and total energy are obtained from the historic data. The random variation of both terms is modeled as a truncated Gaussian distribution that is duration normalized and scaled to the interval -1.1. Only the mean $\mu_{q_{w,m}}$ and standard deviation $\sigma_{q_{w,m}}$ of the truncated Gaussian distributions are parameters because the lower boundary $a_{q_{w,m}} = -1$ is the historic least severe event and the upper boundary $b_{q_{w,m}} = 1$ is the historic most severe event. Here the q index represents total energy and peak extreme temperature ($q = \{\epsilon, \tau\}$). The energy terms are kept constant. The peak temperature's truncated Gaussian distribution mean and standard deviation form the last four parameters over HWs and CSs.

Historic optimization

For each month of the year, a genetic evolutionary algorithm is used by MEWS to fit historic histograms of HW and CS events using the 14 parameters already described. The

definitions of HW and CS events are given in section 2.2.1 of Villa et al. (2023). A least-squares sum of differences between histograms for the MEWS model and historic histograms at a daily scale (i.e., compare results at 1 day, 2 days, etc.) is then computed as the objective function for the optimization. The MEWS model is run for millions of time steps for each month to form a histogram of the stochastic model's outputs.

Shift to future conditions

The same ensemble of CMIP6 model's output of surface temperature ΔT_S was used as for Villa et al. (2023). MEWS takes in latitude and longitude of the site being analyzed to fit a polynomial of ΔT_S versus future year. Specific years are then chosen and the polynomial is evaluated to quantify the shift in peak temperature, ΔT, and multiplier on frequency, Δf, in Table 1 by linear interpolation below 4.0 °C or extrapolation up to 6.05 °C. This value must be adjusted because the preindustrial period 1850–1900 implied by Table 1 is not the same period as the NOAA climate normal or NOAA daily summaries (see Figure 3 of Villa et al. 2023).

For this study, SSP 2–4.5, 3–7.0, and 5–8.5 were used, which required three polynomial fits. These SSPs represent both the most likely outcomes and worst case outcomes for global surface temperature. SSP2–4.5 is a "middle-of-the-road" pathway where trends do not change from historic ones, SSP3–7.0 emphasizes regional rivalry characterized by "resurgent nationalism," and SSP5–8.5 assumes that much of the world's new development will be fossil fuel dependent (O'Neill et al. 2017). The 4.5, 7.0, and 8.5 in the second half of the SSP nomenclature all represent the expected level of radiative forcing in W/m^2 in the year 2100.

For each SSP and future year, six values of ΔT and Δf are obtained from Table 1 for 10- and 50-year events and for 5% and 95% confidence interval (CI) levels from Table 1. Newton's method is then used to shift (i.e., change the mean by $\Delta\mu_{\tau_{w,m}}$) and stretch (i.e., change the standard deviation by $\Delta\sigma_{\tau_{w,m}}$) MEWS's temperature-truncated Gaussian distribution until the 10- and 50-year historically shifted events are least-squares optimally fit. The boundaries of the truncated Gaussian distribution are translated according to the following linear functions:

$$\Delta a_{\tau_{w,m}} = \Delta\mu_{\tau_{w,m}} - \frac{(1+\mu_{\tau_{w,m}})}{\sigma_{\tau_{w,m}}}\Delta\sigma_{\tau_{w,m}} \quad (3)$$

$$\Delta b_{\tau_{w,m}} = \Delta\mu_{\tau_{w,m}} + \frac{(1-\mu_{\tau_{w,m}})}{\sigma_{\tau_{w,m}}}\Delta\sigma_{\tau_{w,m}} \quad (4)$$

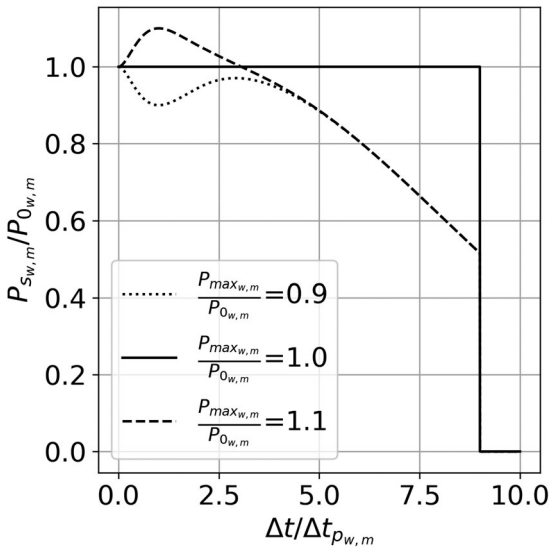

Fig. 2. Time-dependent probability function for HW and CS events.

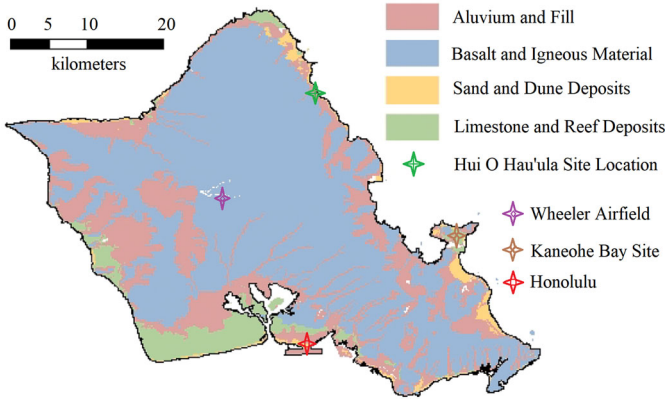

Fig. 3. Major locations and geology of Oahu, Hawaii, adapted from Dores and Lautze with permission (Dores and Lautze 2020).

Table 1. IPCC HW intensity and frequency multiplying factors from Masson-Delmotte et al. (2021, Figure SPM.6).

Event	ΔT_S (ºC)	5% ΔT (ºC)	50% ΔT (ºC)	95% ΔT (ºC)	5% Δf	50% Δf	95% Δf
HW 10-year event	1.0	0.7	1.2	1.5	1.8	2.8	3.2
	1.5	1.3	1.9	2.3	2.8	4.1	4.7
	2.0	1.8	2.6	3.1	3.8	5.6	6
	4.0	4.3	5.1	5.8	8.3	9.4	9.6
HW 50-year event	1.0	0.7	1.2	1.6	2.3	4.8	6.4
	1.5	1.3	2	2.4	4.3	8.6	10.7
	2.0	1.8	2.7	3.2	6.9	13.9	16.6
	4.0	4.4	5.3	6.0	27	39.2	41.4

Surface temperature change is the shift from 1850 to 1900 mean.

Table 2. KCRH design cases used to quantify energy efficiency.

Design aspect	BAU	HE
A/C	Direct expansion (DX) coils for single-duct air terminals with dampers and reheat.	Centralized chilled water coils. Same duct configuration as BAU. High-efficiency variable-speed fans, an outdoor air economizer, and heat exchange between exhaust air and incoming outdoor air. The control includes a supply air temperature reset ranging from 10 to 12°C based on the warmest thermal zone temperature.
Cooling source	DX packaged rooftop unit for heating and cooling with humidity control. No special considerations in efficiently servicing critical loads.	Connected systems: two water source chillers with a ground heat exchanger (GHE) and air-to-water heat rejection. Redundancy for critical loads is provided with either chiller being able to serve them. Also the GHE can reject heat of critical loads without air-to-water heat rejection.
Refrigeration	16 m^2 walk in refrigerator with air-source heat rejection	Connected system: 16-m^2 walk-in refrigeration with water-source heat rejection connected to chiller cooling water (CW) loop
Ventilation	1 common ventilation system, mechanical ventilation in gym	Two ventilation systems fully separating critical and noncritical loads, natural ventilation in gym
Lighting	5 W/m^2 (normal LED performance)	3 W/m^2 (high light-emitting diode [LED] performance with well-coordinated daylighting)
Fans	61% efficiency	80% efficiency
Pumps	90% efficiency	95% efficiency
Walls	1.35 m^2K/W average R value	2.79 m^2-K/W average R value—also interior walls surrounding critical load spaces given exterior insulation for all surfaces
Roof	ASHRAE 189 climate zone 1 exterior roof with 3.9 m^2K/W	Cool roof (solar absorptance of 0.45) with 6.97 m^2-K/W resistivity
Windows	Average U-factor of 4 W/m^2/K, solar heat gain coefficient (SHGC) 0.3, visible light transmittance (VLT) 0.3	Average U-factor of 1 W/m^2-K, SHGC of 0.23, and VLT of 0.4
Doors	25-mm insulation board	R18 (3.2 m^2K/W) + 25 mm insulation board
Waste heat exchange	None	Outside air to exhaust air heat exchanger and sewage water heat recovery
Hot water	Electric element	Heat pump water heater (HPWH) with backup electric element and thick insulation. The HPWH cools mechanical space and indirectly draws waste heat from other equipment.

To obtain both of these models, go to https://github.com/sandialabs/MEWS. Then navigate to "examples," then to "example data," then to "HuiOHauula." The BAU case is in "ep_models" and the HE case is in "ep_models."

Hau'ula KCRH case study

We conducted a study of the proposed KCRH in Hau'ula, HI, using MEWS weather files for extreme heat events. The planned site for the KCRH is near latitude of 21.6113 and longitude of 202.0851 (i.e., −157.9149), as seen at the green star in Figure 3. First the model was created to represent business as usual (BAU), where energy efficiency is code compliant but extra measures to reduce consumption are not taken and thermal sharing between systems is not used. We then reconfigured the model to a high-efficiency (HE) configuration to reduce energy use and to build in capacity to use even less energy for HVAC when a disaster occurs. The BAU and HE cases' design attributes are given in Table 2. The BAU case was only used to verify how much more efficient the HE mode was.

The KCRH HE BEM was then reconfigured to represent how the center will be operated during resilience events (ResOps) in comparison to normal operations (NormOps). The differences between these two modes of operation is provided in Table 3. The objective of the ResOps is to minimize energy use while maximizing medical, water, and food-service capabilities of the center for the surrounding communities. The differences reflect priorities and goals set by the community. For example, cutting all hot water has been an accepted strategy used in the current community center. Also, the occupancy is expected to be 1,500 persons during the sheltering phase of a hurricane, but we assume here that the center will only house critical cases in the 30-day aftermath. Finally, plug loads will have to be rationed during an emergency, with the objective to avoid an increase in plug loads between NormOps and ResOps. Though not

Table 3. Differences between NormOps and ResOps.

Design aspect	NormOps	ResOps
A/C	All spaces cooled except gym, side stairs, mechanical room, and freight elevator	Only cool the following critical spaces: Level 1: kitchen, food storage; Level 2: medical, security; Level 3: staff area, conference room.
Hot water	Available	None
Refrigeration	Walk-in, two stand-alone refrigerators and two stand-alone freezers	Only walk-in
Occupancy	Peak occupancy of 70 people each day with a daily average of 38 people	Four times the occupancy with peak of 282 people and daily average of 153. Gym and critical spaces are occupied at night
Plug loads	11.38 W/m2	Same amount. This implies rationing of plug loads to a larger group of people but with no increase.
Medical	Medical center without dialysis	Medical center + 3 Tablo hemodialysis systems (Tablo 2023) being used during the day (intensive but not 24/7)

Table 4. Changes added to Kane'ohe Bay TMYx 2004–2018 EPW file.

Variable	Change description
Dry-bulb temperature	Optimized offset and multiplicative parameters to match monthly climate average maximum and minimum values from Weather Spark's webpage for Hau'ula to hourly Kane'ohe Bay TMYx (WeatherSpark 2023).
Dew-point temperature	Changed values to be consistent with updated dry-bulb temperature and unchanged relative humidity.
Radiation (direct and diffuse)	Adjusted Kane'ohe Bay TMYx 2004–2018 hourly values so that monthly average, hour-of-day global horizontal radiation values from University of Hawaii (Giambelluca et al. 2014) match for the latitude and longitude of the site.
Ground temperatures	Shifted ground temperatures down by 3.03 °C to make the average of 3-, 4-, and 5-m-deep readings in the TMYx file match ground water temperature of 21.7 °C reported by Dores and Lautze (2020) for Hau'ula

analyzed in this study, the minimization of energy is driven by a desire to keep services available via a microgrid with no support from other power sources for up to 30 days.

Hau'ula climate and weather files

The climate of the Hawaian Islands is very diverse, ranging from dry desert coast land to rainforest climate zones. Hau'ula is directly north of Honolulu on the northeast coast of island of Oahu, as seen at the green star in Figure 3. The northern coast of Oahu is cooler, cloudier, and rainier than the southern coast. The closest coastal NOAA station is the Kane'ohe Bay Marines base, 40 km to the south-east of Hau'ula. Wheeler Airfield is closer but has significantly different climate due to altitude change and being inland. The weather files for Kane'ohe Bay were therefore adjusted for temperature, radiation, and ground temperatures to reconstruct a weather file representative of the local Hau'ula climate. Other important differences including humidity and precipitation do not have sufficient influence on the BEM to require adjustment.

The more recent Typical Meteorological Year Version X (TMYx) 2004–2018 weather file for Kane'ohe Bay was used as the start point for a weather file for Hau'ula (Crawley and Lawrie 2023). Bre et al. (2021) give a thorough description of this newer set of TMY files. Using TMYx files makes more recent climate conditions the baseline for the MEWS analysis. in comparison to Typical Meteorological Year Version 3 (TMY3) files (Wilcox and Marion 2008). This psychrometric file was then adjusted for four variables for which local information was available, as described in Table 4. Though some psychometric radiation/precipitation discrepancies may exist from these adjustments, the shifts were relatively small and the resulting weather patterns are improved to better reflect Hau'ula's climate.

The climate norms and daily summaries required by MEWS used the Kane'ohe Bay information. We therefore assume that the historic HW characteristics are similar for the two locations. This is justified since no other record of temperature exists that allows sufficient information to characterize historic HWs for Hau'ula. Table 5 provides details for the NOAA data.

The Kane'ohe Bay daily summary data had several large gaps, outliers, and many missing values. The outliers were eliminated by cutting out any data that were outside the all-time records for Hawaii temperature range of 10 °C to 38 °C. A seasonal autoregressive integrated moving average

(SARIMA) (1,1,1)(1,1,1,12) model (i.e., all terms first order with monthly seasonality) was used to fill these gaps.

Energy plus model details

The KCRH EnergyPlus model space layout is shown in Figure 4. The model was created in SketchUp with the OpenStudio plug-in and OpenStudio (Trimble 2023; OpenStudio Coalition 2023; DOE 2023b). The center consists of three levels plus an unoccupied ground floor. The ground floor houses covered parking and has stairwell and elevator access to the upper levels. The floor above the ground floor contains a gym, cafeteria, and locker rooms. The main floor contains the entrance, a balcony above the gym, medical area, security/registration area, and classrooms. The uppermost floor has more classrooms, a staff area, and a mechanical room for equipment. Preliminary design drawings provided by + Lab Architect PLLC were used to construct a BEM with 31 thermal zones as seen in Figure 4 (Azaroff 2023). All major features and shading surfaces were included. The plans include a gym, a freight elevator, and a side stairwell that are not air-conditioned. The rest of the building is air-conditioned. Many details for shading were found to have minimal effects on results and were dropped since they significantly increased run time by an order of magnitude.

Table 5. NOAA data characteristics.

Input	Value
Station location	Kane'ohe Bay
Station ID	USW00022519
Climate norms	1991–2020
Daily summaries	1942–2023
Filtering	Daily summaries required gap filling using a SARIMA model

The model was given a range of space type designations, with most of the spaces having an "open office" type space for ASHRAE standard 189.1-2009 for a medium office type (ASHRAE 189.1 2009). All spaces were left with these default space types from OpenStudio except that the kitchen and cafeteria spaces were given schedules and occupancy characteristic of the DOE-prototype full-service restaurant, with some customizations for equipment use (DOE 2023c).

All equipment was kept electric to keep local carbon emissions to zero. A 16-m^2 walk-in refrigerator was installed in the level 1 food storage to enable mass storage of perishable foods. Figure 5 shows how all heat rejection applications are tied into a single loop for the HE model. Details of the equipment size, piping layout, and duct layout were left to EnergyPlus's inference since design details are not yet complete.

An OpenStudio measure was used to alter the number of people being served by the building (Roth, Goldwasser, and Parker 2016). Two EnergyPlus models of the KCRH were therefore created to represent the two modes of operation. The default OpenStudio design days for the Honolulu International Airport were used for all cases. This provides design to hotter conditions (i.e., about 1.0 °C hotter on average) than Hau'ula, adding some conservatism for equipment

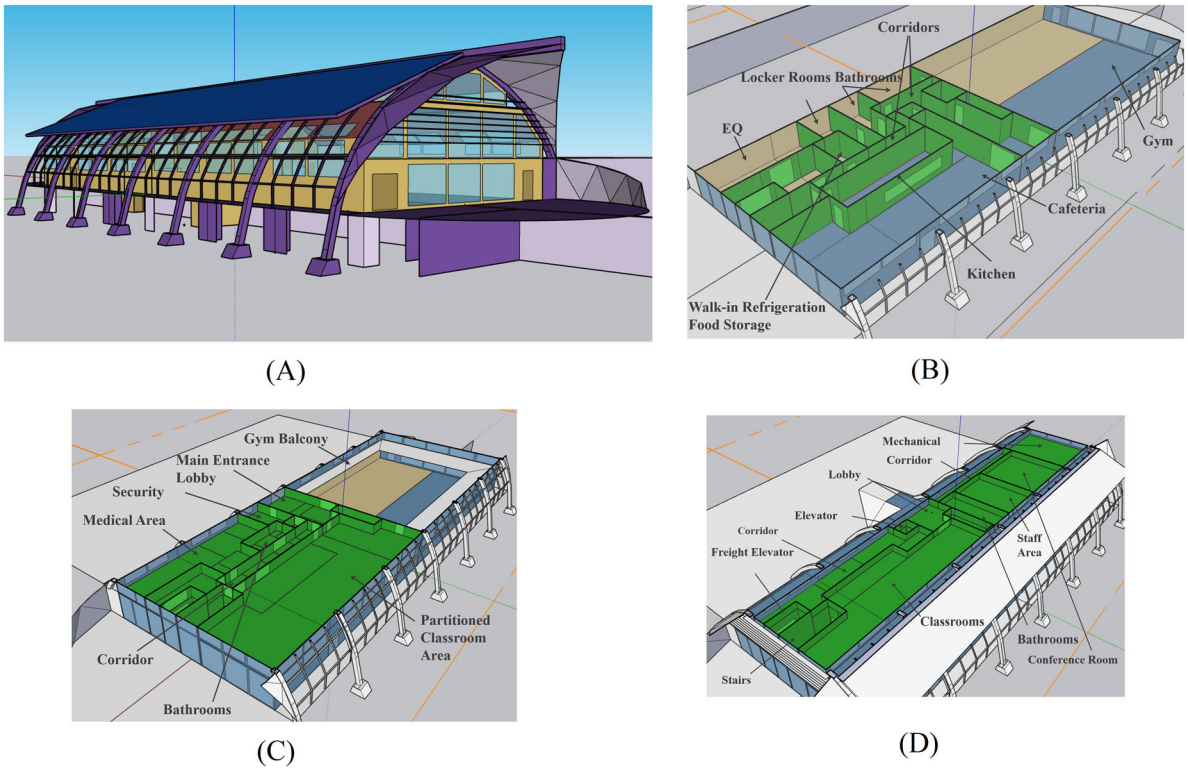

Fig. 4. KCRH in Hau'ula, HI, EnergyPlus model with three levels: (A) isometric view showing covered parking, (B) lower floor, (C) main entrance floor, and (D) upper floor. The design is by + Lab Architect PLLC (Azaroff 2023).

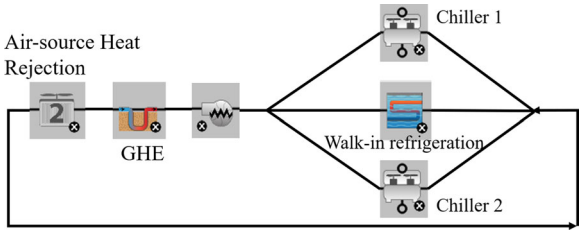

Fig. 5. Shared heat rejection.

sizing. This conservatism decreases as temperature increases in the future. The Honolulu design days are reasonable average design conditions in Hau'ula during the next four decades.

The settings of the model are too extensive to elaborate in full detail here. The models can be downloaded from the MEWS repository example folder in examples/example data/HuiOHauula if the reader desires to use or investigate the model configurations (Villa 2023).

Ground-source heat exchanger

The work of Dores and Lautze (2020) was used to characterize a ground heat exchanger (GHE) for the KCRH. Hau'ula is one of the sites listed as favorable for GHEs. The actual site is marked in Figure 3 and most likely has a subsurface mixture of alluvium, fill, basalt, and igneous material. We used alluvium, to be conservative. We used scenario C (see Tables 3 and 5 of Dores and Lautze [2020]), which represents year-round operation with a lower thermal resistance in the piping. For the alluvium case this leads to an estimated ratio of pipe length to cooling power needed of 0.1374 m/W with 250 kW of cooling needed. We therefore gave a total GHE length of 214 80-m boreholes with supplemental air-source heat rejection for high-temperature periods. This design enables the GHE to fully absorb waste heat during ResOps conditions, while the air-source heat rejection seen in Figure 5 is needed for NormOps.

Results

The MEWS analysis was conducted for the Kane'ohe Bay weather station and the resulting model was applied to the adjusted weather file outlined in the previous section for SSP2–4.5, SSP3–7.0, and SSP5–8.5. EPW files for 2020, 2040, 2060, and 2080 were generated. The extreme values for confidence intervals for HWs (5% and 95%) were included, neglecting the 50% case. The aggregate use of these extreme cases serve as an importance sampling approach to the Monte Carlo study that assures the outer extremes of future HWs are accurately captured. The resulting set of 7,200 files was run on the two operations modes of the KCRH for a total of 14,400 EnergyPlus runs.

MEWS fit

The Kane'ohe Bay daily summary of filtered minimum and maximum temperatures with gaps filled by the SARIMA model is shown in Figure 6. Table 6 shows the

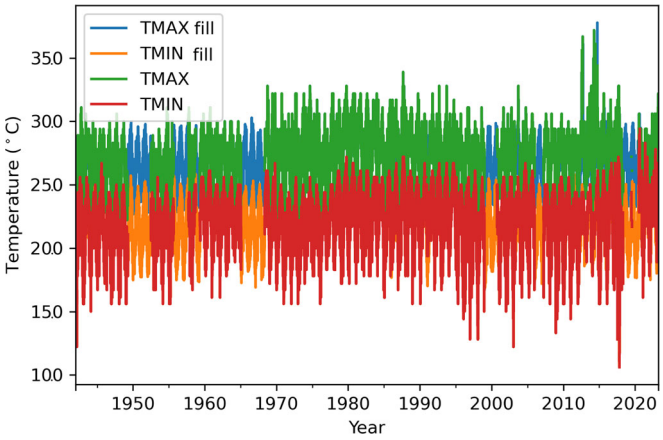

Fig. 6. Gap-filled NOAA daily summaries.

Kolmogorov–Smirnov test results on the MEWS fit. The MEWS HW fit values for duration have 95% confidence for all months except July, August, and November. On the other hand, the temperature distribution fits were not as good as in our previous study (Villa et al. 2023) and only meet 95% confidence for CS in March, May, and December. None of the months for both CSs and HWs meet 95% confidence for both temperature and duration.

Due to the poor Kolmogorov–Smirnov confidence test results shown in Table 6, each month's fit was inspected manually. Figure 7 visualizes this manual inspection for the worst-case p-value month for HWs, June. A graphical view of this month in Figure 7a shows that the fit in June captures the majority of most extreme heat events. Similarly for the other months, none of the poor results disqualified use of the MEWS fit.

Though not captured by the MEWS fit, the absolute extreme event of 11 °C is the basis for the IPCC shift from historical 10- and 50-year events which causes HWs to greatly exceed historic HWs by 2080 as seen in the distribution for 95% IPCC HW confidence interval (CI), SSP 5–8.5 in Figure 7b. Figure 7b shows results for the shift procedure. The arrows show the temperature offset from the historic 10-year (purple-dashed) and 50-year (green-dashed) events to new future targets (blue- and red-dashed). The orange distribution is the future MEWS distribution with 10- and 50-year events that are least-squares optimally fit via Newton's method to occur Δf more times with ΔT greater temperature from the historic value (both from Table 1). The gap between the dotted and dashed blue lines is the temperature error for the 10-year event, and the gap between the dotted and dashed red lines is the 50-year event error. Figure 7c shows the duration fits for June, which passed the Kolmogorov–Smirnov test with 95% confidence.

The polynomial fits to CMIP6 surface temperature that drive the HW intensity and frequency change parameters in Table 1 are shown in Figure 8. It is notable that Hawaii does not have nearly as much increase in temperature as our previous Worcester, MA, study (Villa et al. 2023). This is expected since Hawaii is at a much lower latitude and global warming rates are much greater to the north. Table 7

Table 6. Kolmogorov–Smirnov test statistics for MEWS Kane'ohe Bay fit.

	Duration				Temperature			
	HW		CS		HW		CS	
Month	Statistic	*p* Value	Statistic	*p* Value	Statistic	*p* Value	Statistic	*p* Value
1	0.023092	0.999775	0.115327	0.001477	0.200695	7.456524e-08	0.157785	0.000003
2	0.078382	0.230246	0.114468	0.004146	0.137200	2.811642e-03	0.124873	0.001286
3	0.070624	0.379734	0.094384	0.008577	0.170377	1.474030e-04	0.076134	0.057162
4	0.086225	0.192003	0.070097	0.069220	0.138662	4.877060e-03	0.114668	0.000255
5	0.068583	0.403028	0.092746	0.006257	0.112478	2.867868e-02	0.059037	0.190783
6	0.093537	0.159609	0.070157	0.078387	0.250759	2.765237e-08	0.139464	0.000006
7	0.131092	0.002089	0.059334	0.181783	0.196401	4.047055e-07	0.096573	0.003609
8	0.111761	0.011250	0.127836	0.000047	0.199154	1.443825e-07	0.123753	0.000091
9	0.120070	0.062826	0.084999	0.009526	0.173652	1.478366e-03	0.136081	0.000002
10	0.078358	0.172331	0.089130	0.005178	0.138592	9.849804e-04	0.123505	0.000022
11	0.103622	0.021321	0.045475	0.481458	0.100676	2.746377e-02	0.105592	0.001085
12	0.087386	0.072944	0.090776	0.023918	0.142417	3.144755e-04	0.074269	0.102565

Ninety-five percent confidence is equivalent to the p value being greater than 0.05. Values failing the test are shown in red. The "Statistic" columns give the maximum difference in cumulative distribution functions of the historic distribution versus the MEWS fit.

provides the coefficient values for all four polynomial fits with a higher order polynomial required for the historic fit back to 1850.

The histograms of the statistical moments for the 7,200 weather files produced by MEWS are shown in Figure 9. The maximum temperatures exceed Hawaii's record of 38 °C for quite a few cases.

EnergyPlus model verification

The EUI calculated for the adjusted TMYx weather file for the HE case against the BAU configuration of the model is shown in Table 8. Table 9 provides a comparative basis with EUI benchmarks for several categories of buildings in Hawaii that share attributes with the KCRH.

Thermal resilience

The thermal resilience of the KCRH is highly dependent on the mode of operation. The NormOps and ResOps modes provide a trade-off between thermal resilience and energy savings. Figure 10 shows how thermal resilience decreases into the future for ResOps on the left and NormOps on the right. The x axis portrays the average percent of hours across all 31 BEM thermal zones for four thermal ranges of indoor air temperature (C = caution, 32.2 °C $< T \leq$ 26.7 °C; D = danger, 32.2 °C $< T \leq$ 39.4 °C; EC = extreme caution, 39.2 °C $< T \leq$ 51.7 °C; ED = extreme danger, $T >$ 51.7 °C). Here, the average is applied across the 31 thermal zones in the KCRH BEM. The violin plot shows how gradual temperature rise from 2020 to 2080 affects the thermal resilience through the different color probability distributions that shift to the right. It also shows how extreme events spread out the average outcome via the minimum and maximum bars to the left and right of each distribution.

Figure 11 shows EUI as a function of year, mode of operation, and SSP. Figure 12 combines these two issues with average dangerous hours versus total cooling electrical energy.

Discussion

The MEWS approach is important because dynamic downscaling methods (CORDEX 2021) would require prohibitively large numbers of climate model runs to adopt a stochastic methodology within BEM analysis. Keeping a regional climate model in the loop for such analysis is not practical. Our approach therefore enables stochastic extreme temperatures for BEM such that resilience can be fully assessed given an uncertain future. This is especially true if events such as power outages need to be evaluated alongside weather changes. Alternative approaches to ours exist, such as that of Yassaghi, Gurian, and Hoque (2020), where energy modeling results for future climate are extrapolated. This approach has some advantages over ours because it does not require a full Monte Carlo analysis and a stochastic weather generator like MEWS. It cannot capture the kinds of changes in operations to the buildings that we have analyzed, though, and does not consider FDI changes to extreme heat. Another approach, given by Zhuang, Choudhary, and Mavrogianni (2023), investigates the efficacy of energy retrofits with a hybrid of (1) selected Global Circulation Model (GCM) results closest to historic data and (2) morphing (Belcher, Hacker, and Powell 2005) to future conditions. This approach contains uncertainty across GCMs but does not systematically consider uncertainty. Additional stochastic approaches to climate uncertainty in energy models are abundant in the literature and are not discussed here in detail. A good review of this subject is available by Plaga and Bertsch (2023).

A better fit from MEWS is desirable, but the visual inspections performed via figures like Figure 7 clearly show that the analysis is conservative with respect to projected

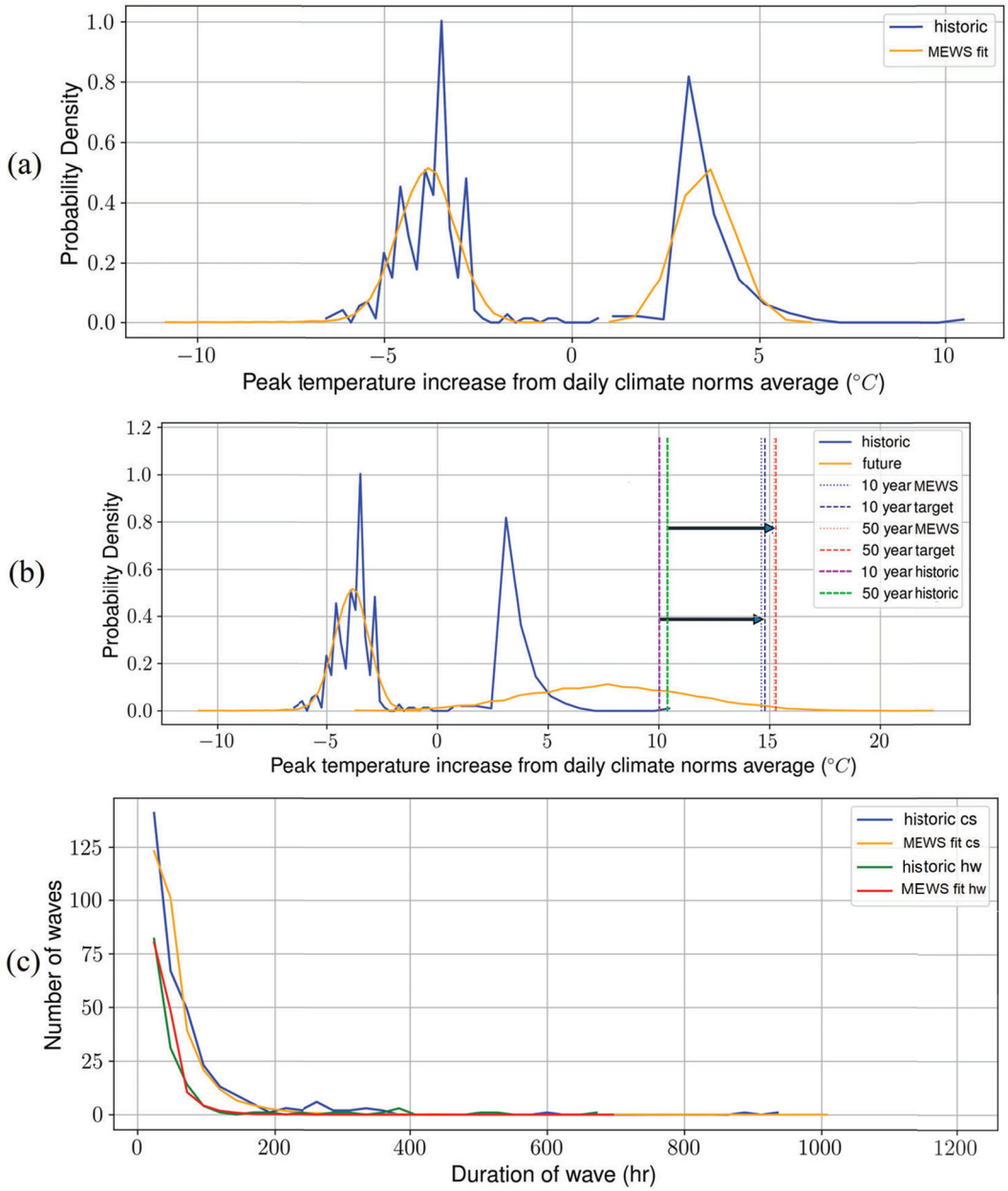

Fig. 7. June MEWS fits to temperature (a) and duration (c) and shift and stretch for SSP 5–8.5 for 2080 and 95% HW CI (b).

extreme HWs according to IPCC (Masson-Delmotte et al. 2021). Even so, these are only projections based on the best information available today. The actual changes in climate for Hawaii could exceed the interval analyzed.

Though no calibration target was set by the design team, the data in Tables 8 and 9 indicate that the KCRH EnergyPlus models have reasonable levels of energy consumption. The KCRH has a combination of office space, conference rooms, and classrooms that should be expected to perform similar to office buildings. A slight increase in EUI is expected though because of the cafeteria, kitchen, and walk-in refrigeration that make it a hybrid of the four building types in Table 9. The presence of facilities without A/C in Hawaii makes the minimum values for the HEUB data good comparisons for the ResOps mode of operation.

The results of the Monte Carlo study shown in Figures 10–12 enable quantifiable trade-offs that can answer our research questions. There is a clear increase in loss of thermal resilience for both modes of operation. Cutting A/C for the ResOps mode amplifies this loss of thermal resilience on average by a factor of five. The sensitivity of thermal resilience outcomes is especially pronounced for SSP 5–8.5. Conversely, the EUI is negligibly sensitive to future conditions since the A/C is cut for the ResOps mode. The NormOps mode has a clear trend but the increase is at maximum 0.8% change in EUI. The climate trends are not present for the ResOps mode, as seen on the left-hand side of Figure 11. This is evident in Figure 12, where the spread in thermally dangerous hours increases with later years but the cooling load does not increase. This indicates that most of

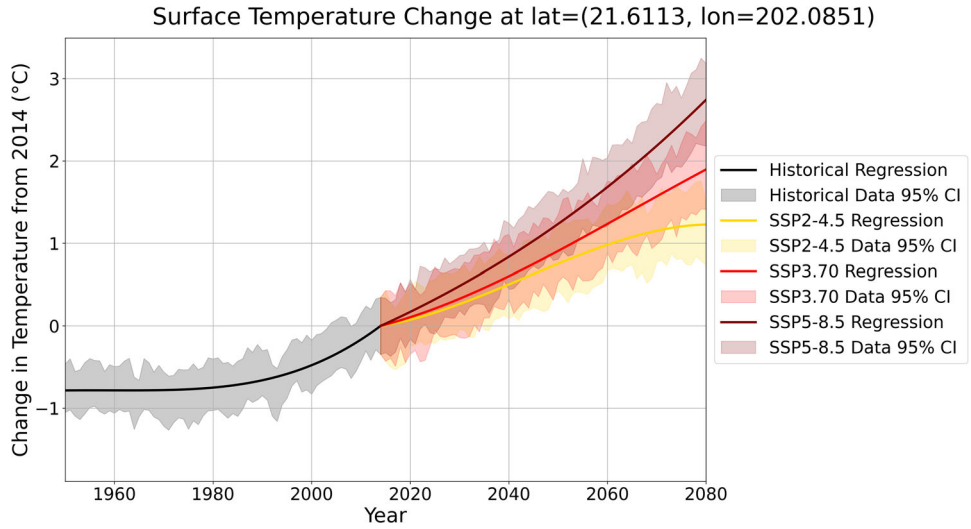

Fig. 8. CMIP6 polynomial fits to surface temperature at the KCRH site.

Table 7. CMIP6 polynomial coefficients t = year − 2014.

	t^6	t^5	t^4	t^3	t^2	t	1
Historical	−1.8231e-12	−7.0498e-10	−7.2341e-08	2.6166e-06	8.2021e-04	4.4934e-02	−4.7280e-06
SSP2-4.5	0	0	0	−5.9508e-06	5.2949e-04	9.5840e-03	−2.2866e-07
SSP3-7.0	0	0	0	−2.3118e-06	3.5316e-04	1.5495e-02	−2.2594e-07
SSP5-8.5	0	0	0	7.1558e-07	1.6873e-04	2.7302e-02	−7.8113e-08

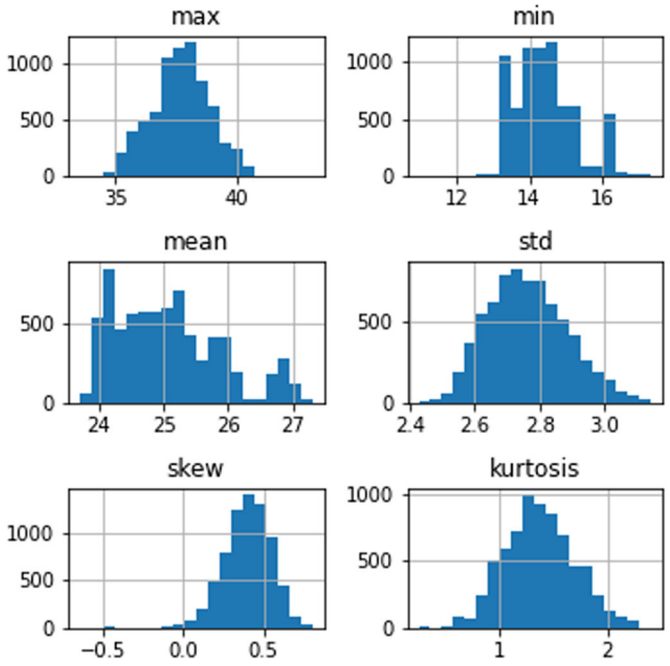

Fig. 9. Statistical moments of dry-bulb temperature (°C) for 7,200 weather files. The x axis is °C or Δ°C for all plots.

the change in thermal resilience is in spaces not air-conditioned. Increased A/C load from climate change in Hau'ula is therefore not very large for our study. A combination of the mild climate, less sensitivity to climate change at Hawaii's latitude, and the fact that equipment simply cannot sufficiently cool the facility for extreme events with the constant design day used leads to the minor differences in cooling energy. On the other hand, the consequence of not having more cooling capacity for extreme events is increasing the hours of exposure to dangerous conditions with much more sensitivity.

Though the decrease in thermal resilience is not desirable, dropping A/C loads to save energy for ResOps is still acceptable. Several factors support this: (1) The most important climatic shock event is a hurricane, which brings significant cooling, making extreme heat less relevant for a couple of weeks. (2) Appropriate contingency planning can overcome thermally hot conditions in the facilities. There is still air-conditioned space in the KCRH. In worst-case scenarios where dangerous temperatures exist, staff in charge of the KCRH can prioritize access to this air-conditioned space for individuals who are heat stressed. In addition, the walk-in refrigeration capacity is supported for the ResOps mode and chilled drinks and ice can be available onsite for aiding thermal comfort of the surrounding population that is not in distress. (3) External conditions in Hawaii are hot and humid but seldom dangerously hot for healthy resting individuals. Even the most extreme futures generated by MEWS seen in Figure 9 are survivable. We therefore conclude that all thermal resilience concerns for the ResOps mode of the KCRH can be overcome if (1) thermally distressed individuals can be given prioritized access to A/C and (2) the microgrid-supported, 16-m^2 walk-in refrigeration unit includes capacity to cool drinks for up to 1,500 people for 3 days and for 282 people for 30 days. It is likely that the same conclusion

Table 8. EUI results for all four models.

EUI (1915 m^2), kWh/m^2/yr	Business-as-usual configuration (BAU)	High-efficiency configuration (HE)	Energy savings (%)
NormOps	189.95	118.92	37.39
ResOps	122.20	90.32	26.07

Table 9. Hawai'i Energy Utility Benchmarking (HEUB) data (HEUB 2023).

EUI, kWh/m^2/yr	Minimum	Average	Maximum	Number of samples
Grocery stores	129	530	690	33
Office buildings	86	170	290	60
Restaurants	48	350	650	14
Hotels	21	110	200	27

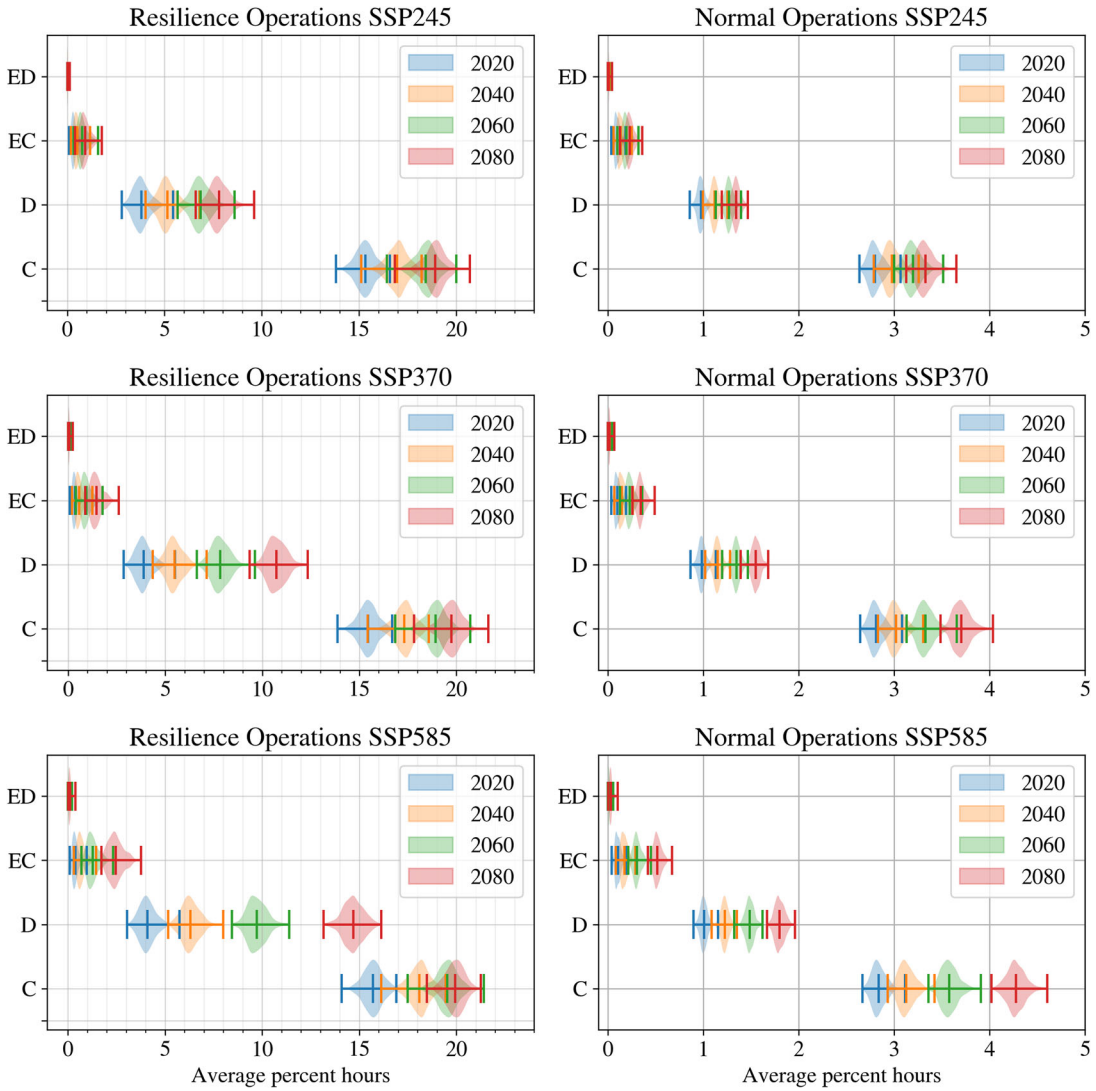

Fig. 10. Average percent hours within four temperature ranges. C = caution, 32.2 °C < $T \leq$ 26.7 °C; D = danger, 32.2 °C < $T \leq$ 39.4 °C; EC = extreme caution, 39.2 °C < $T \leq$ 51.7 °C; ED = EXTREME Danger, $T >$ 51.7 °C. Rows vary by SSP and columns by operation type.

Fig. 11. EUI by operation mode, year, and SSP (colors according to legend in Figure 9). The y axis is probability density.

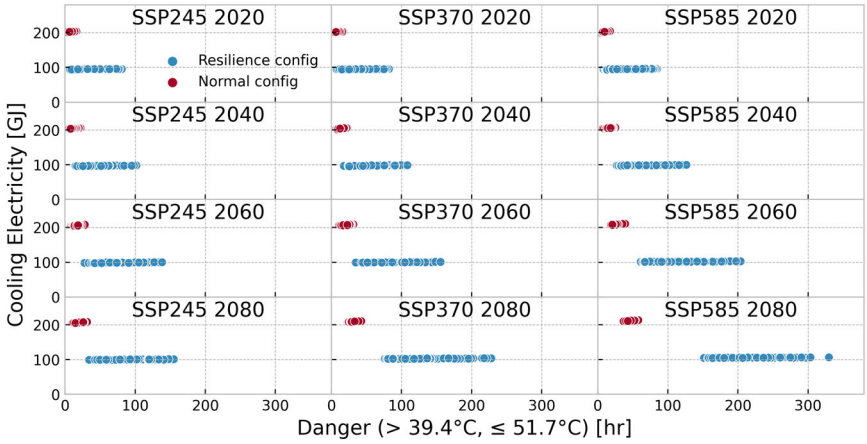

Fig. 12. Cooling energy vs. average dangerous hours by operation mode, year, and SSP.

concerning thermal resilience of buildings can be drawn for other locations of similar climate and building characteristics. In short, increases in FDI for HWs for the KCRH design do not sufficiently affect outcomes to make building-wide A/C a requirement for future survival. Hau'ula's present and future climates therefore leave room for gaining the significant benefits of the ResOps mode as defined in Table 3. This will result in a smaller microgrid than would be needed for only having the NormOps mode. The cost benefits from needing a smaller microgrid may cover a significant amount of the additional cost needed to support the HE design that specializes A/C for ResOps.

Conclusions

MEWS algorithms for HWs and a case study for the future KCRH in Hau'ula, Hawaii have been presented in this article. The results show that decreased thermal resilience is significant due to global warming and increased FDI of HWs. Regardless, Hau'ula's future worst-case HWs produced by MEWS to 2080 do not produce conditions that make A/C mandatory for healthy individuals. The decreased thermal resilience for the KCRH can therefore be overcome through other means than providing A/C to the entire KCRH. The decreased energy consumption provided by the ResOps mode is therefore worth gaining. Even so, there are five times more average percent hours above temperature ranges of concern within spaces in the KCRH. The decreases in energy use gained by cutting A/C in the KCRH must therefore be balanced with planning to ensure air-conditioned space is given to anyone in thermal distress. Our study gives an example of how multi-operations-mode building systems can become part of assuring adaptation to climate change and extreme weather events in humanity's future. Further research is needed to show how well multi-operations-mode building systems enable adaptation to climate change and other design basis threats besides heat waves such as hurricanes and earthquakes (Villa and Quiroz 2023). This needs to be done in a broad region-wide context to provide stronger conclusions about what scenarios are the most important and what adaptation measures are most effective.

The MEWS tool has been enhanced since our previous work through a parameter optimization scheme that handles changes to FDI of HWs to 2080 (Villa et al. 2022, 2023). Continued development of MEWS could further enhance its capabilities. The most important next step is to show how MEWS analyses produce nearly equivalent results when temperature histories from climate model reanalysis of historic conditions are used instead of the NOAA data. If this is established, then climate model reanalysis could be used to create a much more comprehensive weather alteration than the dry-bulb temperature alteration made in this study. Stochastic models of humidity, solar radiation, cloud cover, and other variables could be constructed based on signals for each extreme heat event. Regardless, the current MEWS approach captures most of the variation for boundary conditions for BEM and provides a good assessment of building energy usage and thermal comfort performance evaluation for changes to FDI of future HWs.

Acknowledgment

Thanks to Mike Campton from National Renewable Energy Laboratory for coordination of the Hau'ula ETIPP project and to the Hui O Hau'ula community team led by Dotty Kelly-Paddock.

Disclaimer

Sandia National Laboratories is a multimission laboratory managed and operated by National Technology and Engineering Solutions of Sandia, LLC., a wholly owned subsidiary of Honeywell International, Inc., for the U.S. Department of Energy's National Nuclear Security Administration under contract DE-NA0003525. This article describes objective technical results and analysis. Any subjective views or opinions that might be expressed in the article do not necessarily represent the views of the U.S. Department of Energy or the U.S. government.

Disclosure statement

No potential conflict of interest was reported by the author(s).

Funding

This work was funded by U.S. Department of Energy (DOE) DOE Building Technologies Office (BTO) Future Weather Project (BTO 2023) and supported by DOE's Energy Transitions Initiative Partnership Project (ETIPP) project for Hau'ula, Hawaii under contract number NL0039169.

ORCID

Daniel L. Villa http://orcid.org/0000-0001-5339-4902

References

Abadie, L. M., A. Chiabai, and M. B. Neumann. 2019. Stochastic diffusion models to describe the evolution of annual heatwave statistics: A three-factor model with risk calculations. *The Science of the Total Environment* 646:670–84. doi: 10.1016/j.scitotenv.2018.07.158.

Adelard, L., T. A. Mara, H. Boyer, and J. C. Gatina. 2012. Elaboration of a new tool for weather data sequences generation. arXiv preprint arXiv:1212.5599. doi: 10.48550/arXiv.1212.5599

Aguiar, R., S. Camelo, and H. Goncalves. 1999. Assessing the value of typical meteorological years built from observed and from synthetic data for building thermal simulation. Proceedings of Building Simulation 1999: 6th Conference of IBPSA BS 1999 Kyoto, Japan, September 13–15, Vol. 2. Citeseer, 627–34. doi: 10.26868/25222708.1999.A-27

Akkose, G., C. M. Akgul, and I. G. Dino. 2021. Educational building retrofit under climate change and urban heat island effect. *Journal of Building Engineering* 40 (AUG):102294. doi: 10.1016/j.jobe.2021.102294.

ASHRAE. 2017. ANSI/ASHRAE Standard 55-2017, Thermal environmental conditions for human occupancy. ASHRAE Standard, ASHRAE, Atlanta, GA.

ASHRAE 189.1. 2009, March. Standard for the design of high-performance, green buildings except low-rise residential buildings. Standard, ASHRAE, Atlanta, GA.

Attia, S., R. Levinson, E. Ndongo, P. Holzer, O. Berk Kazanci, S. Homaei, C. Zhang, B. W. Olesen, D. Qi, M. Hamdy, et al. 2021. Resilient cooling of buildings to protect against heat waves and power outages: Key concepts and definition. *Energy and Buildings* 239:110869. doi: 10.1016/j.enbuild.2021.110869.

Azaroff, I. 2023. +Lab Architect PLLC website. https://www.pluslabglobal.com/.

Bass, B., and J. New. 2023. How will United States commercial building energy use be impacted by IPCC climate scenarios? *Energy* 263:125945. doi: 10.1016/j.energy.2022.125945.

Bass, B., J. New, and Z. Wade. 2022, November. Future typical meteorological year (fTMY) weather data and climate change impacts to Maricopa county, Arizona. BuildSys'22 Proceedings of the 9th ACM International Conference on Systems for Energy-Efficient Buildings, Cities, and Transportation, November 9–10. Boston, MA: Association for Computing Machinery, 504–7. https://www.osti.gov/servlets/purl/1898988.

Bekris, Y., P. C. Loikith, and J. D. Neelin. 2023. Short warm distribution tails accelerate the increase of humid-heat extremes under global warming. *Geophysical Research Letters* 50 (11): e2022GL102164. doi: 10.1029/2022GL102164.

Belcher, S. E., J. N. Hacker, and D. S. Powell. 2005. Constructing design weather data for future climates. *Building Services Engineering Research and Technology* 26 (1):49–61. doi: 10.1191/0143624405bt112oa.

Bianchi, C., and A. D. Smith. 2019. Localized Actual Meteorological Year File Creator (LAF): A tool for using locally observed weather data in building energy simulations. *SoftwareX* 10: 100299. doi: 10.1016/j.softx.2019.100299.

Brackney, L., A. Parker, D. Macumber, and K. Benne. 2018. *Building energy modeling with OpenStudio: A practical guide for students and professionals*. Cham: Springer. doi: 10.1007/978-3-319-77809-9

Bre, F., R. M. e Silva Machado, L. K. Lawrie, D. B. Crawley, and R. Lamberts. 2021. Assessment of solar radiation data quality in typical meteorological years and its influence on the building performance simulation. *Energy and Buildings* 250:111251. doi: 10.1016/j.enbuild.2021.111251.

BTO. 2023. Building Technologies Office Future weather project website. https://www.energy.gov/eere/buildings/femy-future-and-extremeweather-data.

Cabeza, L. F., and M. Chafer. 2020. Technological options and strategies towards zero energy buildings contributing to climate change mitigation: A systematic review. *Energy and Buildings* 219 (JUL 15):110009. doi: 10.1016/j.enbuild.2020.110009.

Chen, Y., M. Guo, Z. Chen, Z. Chen, and Y. Ji. 2022. Physical energy and data-driven models in building energy prediction: A review. *Energy Reports* 8:2656–71. doi: 10.1016/j.egyr.2022.01.162.

Cohen, J., X. Zhang, J. Francis, T. Jung, R. Kwok, J. Overland, T. J. Ballinger, U. S. Bhatt, H. W. Chen, D. Coumou, et al. 2020. Divergent consensuses on Arctic amplification influence on midlatitude severe winter weather. *Nature Climate Change* 10 (1): 20–9. doi: 10.1038/s41558-019-0662-y.

CORDEX. 2021. Coordinated Regional Climate Downscaling Experiment (CORDEX) website. https://cordex.org/.

Cowan, T., A. Purich, S. Perkins, A. Pezza, G. Boschat, and K. Sadler. 2014. More frequent, longer, and hotter heat waves for Australia in the twenty-first century. *Journal of Climate* 27 (15):5851–71. doi: 10.1175/JCLI-D-14-00092.1.

Crawley, D. B., and L. K. Lawrie. 2023. TMYx weather database. https://climate.onebuilding.org/.

D'Agostino, D., D. Parker, I. Epifani, D. Crawley, and L. Lawrie. 2022. How will future climate impact the design and performance of nearly zero energy buildings (NZEBs)? *Energy* 240:122479. doi: 10.1016/j.energy.2021.122479.

De la Pena, L., R. Guo, X. Cao, X. Ni, and W. Zhang. 2022. Accelerating the energy transition to achieve carbon neutrality. *Resources Conservation and Recycling* 177 (FEB):105957. doi: 10.1016/j.resconrec.2021.105957.

De Masi, R. F., A. Gigante, S. Ruggiero, and G. P. Vanoli. 2021. Impact of weather data and climate change projections in the refurbishment design of residential buildings in cooling dominated climate. *Applied Energy* 303:117584. doi: 10.1016/j.apenergy.2021.117584.

DOE. 2023a. EnergyPlus website. Accessed 8/4/2023. https://energyplus.net/.

DOE. 2023b. OpenStudio Website. Accessed 8/4/2023. https://http://openstudio.net/.

DOE. 2023c. DOE prototype model website. Accessed 8/4/2023. https://www.energycodes.gov/sites/default/files/2020-06/ASHRAE901_RestaurantSitDown.zip.

Dores, D., and N. Lautze. 2020. Preliminary assessment of ground-source heat exchangers for cooling in Hawai'i. *Sustainable Energy Technologies and Assessments* 37:100579. doi: 10.1016/j.seta.2019.100579.

Farah, S., W. Saman, and J. Boland. 2018. Development of robust meteorological year weather data. *Renewable Energy.*118:343–50. doi: 10.1016/j.renene.2017.11.033.

FEMA. 2021a, April. Safe rooms for tornadoes and hurricanes: Guidance for community and residential safe rooms FEMA P-361. Technical Report, FEMA, Washington, DC. https://www.fema.gov/sites/default/files/documents/fema_safe-rooms-for-tornadoes-and-hurricanes_p-361.pdf.

FEMA. 2021b, March. Taking shelter from the storm: Building or installing a safe room for your home (includes design plans) FEMA P-320. Technical Report, FEMA, Washington, DC. https://www.fema.gov/sites/default/files/documents/fema_taking-shelter-from-the-storm_p-320.pdf.

Fonseca, J. A., I. Nevat, and G. W. Peters. 2020. Quantifying the uncertain effects of climate change on building energy consumption across the United States. *Applied Energy* 277: 115556. doi: 10.1016/j.apenergy.2020.115556.

Giambelluca, T. W., X. Shuai, M. L. Barnes, R. J. Alliss, R. J. Longman, T. Miura, Q. Chen, A. G. Frazier, R. G. Mudd, L. Cuo, et al. 2014, February. Evapotranspiration of Hawai'i. Final report submitted to the U.S. Army Corps of Engineers—Honolulu District, and the Commission on Water Resource Management, State of Hawai'i. Technical Report. http://evapotranspiration.geography.hawaii.edu/assets/files/PDF/ET%20Project%20Final%20Report.pdf.

Grossman-Clarke, S., S. Schubert, T. R. Clarke, and S. L. Harlan. 2014. Extreme summer heat in Phoenix, Arizona (USA) under global climate change (2041-2070). *ERDE* 145 (1-2):49–61. https://www.die-erde.org/index.php/die-erde/article/view/92/60.

HEUB. 2023. Hawai'i Energy Utility Benchmarking data website. https://hawaiienergy.com/for-business/benchmarking-by-facility-type.

Hirsch and Associates. 2023. DOE-2 website. http://www.doe2.com/.

Hong, Y., S.-Y S. Wang, S.-W. Son, J.-H. Jeong, S.-W. Kim, B. Kim, H. Kim, and J.-H. Yoon. 2023. Arctic-associated increased fluctuations of midlatitude winter temperature in the 1.5° and 2.0° warmer world. *NPJ Climate and Atmospheric Science* 6 (1). doi: 10.1038/s41612-023-00345-y.

Hosseini, M., F. Tardy, and B. Lee. 2018. Cooling and heating energy performance of a building with a variety of roof designs; the effects of future weather data in a cold climate. *Journal of Building Engineering* 17 (MAY):107–14. doi: 10.1016/j.jobe.2018.02.001.

Hausfather, Z. 2018. Explainer: How scientists estimate climate sensitivity. Carbon Brief. https://www.carbonbrief.org/explainer-how-scientistsestimate-climate-sensitivity.

IEA. 2019. 2019 global status report for buildings and construction: Toward a zero emissions, efficient and resilient buildings and construction sector. Technical Report. https://www.iea.org/reports/global-status-report-for-buildings-and-construction-2019.

Keellings, D., and H. Moradkhani. 2020. Spatiotemporal evolution of heat wave severity and coverage across the United States. *Geophysical Research Letters* 47 (9):e2020GL087097. doi: 10.1029/2020GL087097.

Koci, J., V. Koci, J. Madera, and R. Cerny. 2019. Effect of applied weather data sets in simulation of building energy demands:

Comparison of design years with recent weather data. *Renewable & Sustainable Energy Reviews* 100:22–32. doi: 10.1016/j.rser.2018.10.022.

Lee, C.-C., M. Maron, and A. Mostafavi. 2022. Community-scale big data reveals disparate impacts of the Texas winter storm of 2021 and its managed power outage. *Humanities and Social Sciences Communications* 9 (1):335. doi: 10.1057/s41599-022-01353-8.

Lokeshgupta, B., and K. Ravivarma. 2023. Coordinated smart home energy sharing with a centralized neighbourhood energy management. *Sustainable Cities and Society* 96:104642. doi: 10.1016/j.scs.2023.104642.

Masson-Delmotte, V., P. Zhai, A. Pirani, S. L. Connors, C. Péan, S. Berger, N. Caud, Y. Chen, L. Goldfarb, M. I. Gomis, et al., eds. 2021. Technical summary. In *Climate change 2021: The Physical science basis. Contribution of working group I to the sixth assessment report of the Intergovernmental Panel on Climate Change*, 135–144. Cambridge, UK: Cambridge University Press. doi: 10.1017/9781009157896.002.

Mathew, P., L. Sanchez, S. Lee, and T. Walter. 2021. Assessing the energy resilience of office buildings: Development and testing of a simplified metric for real estate stakeholders. *Buildings* 11 (3):96. doi: 10.3390/buildings11030096.

Meehl, G. A., C. Tebaldi, S. Tilmes, J.-F. Lamarque, S. Bates, A. Pendergrass, and D. Lombardozzi. 2018. Future heat waves and surface ozone. *Environmental Research Letters* 13 (6):064004. doi: 10.1088/1748-9326/aabcdc.

Munankarmi, P., J. Maguire, S. P. Balamurugan, M. Blonsky, D. Roberts, and X. Jin. 2021. Community-scale interaction of energy efficiency and demand flexibility in residential buildings. *Applied Energy* 298:117149. doi: 10.1016/j.apenergy.2021.117149.

NOAA. 2021a. Global Historical Climatology Network daily (GHCNd) version 3.28-upd-2021100417, National Oceanic and Atmospheric Association. https://www.ncei.noaa.gov/data/daily-summaries/access/.

NOAA. 2021b. U.S. climate normals for 1991-2020. https://www.ncei.noaa.gov/data/normals-hourly/1991-2020/access/.

OpenStudio Coalition. 2023. OpenStudio Coalition website. https://openstudiocoalition.org/.

O'Neill, B. C., E. Kriegler, K. L. Ebi, E. Kemp-Benedict, K. Riahi, D. S. Rothman, B. J. van Ruijven, D. P. van Vuuren, J. Birkmann, K. Kok, et al. 2017. The roads ahead: Narratives for shared socioeconomic pathways describing world futures in the 21st century. *Global Environmental Change* 42:169–80. doi: 10.1016/j.gloenvcha.2015.01.004.

Plaga, L. S., and V. Bertsch. 2023. Methods for assessing climate uncertainty in energy system models—A systematic literature review. *Applied Energy* 331:120384. doi: 10.1016/j.apenergy.2022.120384.

Ragone, F., J. Wouters, and F. Bouchet. 2018. Computation of extreme heat waves in climate models using a large deviation algorithm. *Proceedings of the National Academy of Sciences of the United States of America* 115 (1):24–9. doi: 10.1073/pnas.1712645115.

Rahif, R., D. Amaripadath, and S. Attia. 2021. Review on time-integrated overheating evaluation methods for residential buildings in temperate climates of Europe. *Energy and Buildings* 252:111463. doi: 10.1016/j.enbuild.2021.111463.

Rastogi, P., and M. Andersen. 2015. Embedding stochasticity in building simulation through synthetic weather files. Proceedings of Building Simulation 2015: 14th Conference of IBPSA, Vol. 14, Building Simulation, Hyderabad, India, December 7–9, 963–70. doi: 10.26868/25222708.2015.2321

Rastogi, P., and M. Andersen. 2016. "Incorporating climate change predictions in the analysis of weather-based uncertainty." ASHRAE and IBPSA-USA SimBuild 2016–Building Performance Modeling Conference. IBPSA-USA, ASHRAE. https://publications.ibpsa.org/conference/paper/?id=simbuild2016_C024.

Rastogi, P., and M. E. Khan. 2021. Planning for a changing climate without accurate predictions. In *Climate adaptation and resilience across scales*, 35–49. Routledge. doi: 10.4324/9781003030720

Rastogi, P., M. E. Khan, and M. Andersen. 2022. Evaluating the suitability of regression-based emulators of building performance in practice: A test suite. *Journal of Building Performance Simulation* 15 (4):488–506. doi: 10.1080/19401493.2021.1969430.

Roth, A., D. Goldwasser, and A. Parker. 2016. There's a measure for that!. *Energy and Buildings* 117:321–31. doi: 10.1016/j.enbuild.2015.09.056.

Semenov, M. A., and E. M. Barrow. 2002. LARS-WG: A stochastic weather generator for use in climate impact studies. User Manual Herts UK. http://resources.rothamsted.ac.uk/sites/default/files/groups/mas-models/download/LARS-WG-Manual.pdf.

Siu, C. Y., and Z. Liao. 2020. Is building energy simulation based on TMY representative: A comparative simulation study on doe reference buildings in Toronto with typical year and historical year type weather files. *Energy and Buildings* 211:109760. doi: 10.1016/j.enbuild.2020.109760.

Sun, K., M. Specian, and T. Hong. 2020. Nexus of thermal resilience and energy efficiency in buildings: A case study of a nursing home. *Building and Environment* 177:106842. doi: 10.1016/j.buildenv.2020.106842.

Sylla, M. B., F. Giorgi, P. M. Ruti, S. Calmanti, and A. Dell'Aquila. 2011. The impact of deep convection on the West African summer monsoon climate: A regional climate model sensitivity study. *Quarterly Journal of the Royal Meteorological Society* 137 (659):1417–30. doi: 10.1002/qj.853.

Tablo. 2023. Tablo hemodialysis unit web page. Accessed June 6, 2023. https://www.outsetmedical.com/tablo.

Trimble. 2023. SketchUp website. http://www.sketchup.com.

Villa, D. 2023. Multi-scenario Extreme Weather Simulator GitHub repository. https://github.com/sandialabs/MEWS.

Villa, D. L. 2021. Institutional heat wave analysis by building energy modeling fleet and meter data. *Energy and Buildings* 237:110774. doi: 10.1016/j.enbuild.2021.110774.

Villa, D. L., J. Pablo Carvallo, C. Bianchi, and S. Hoon Lee. 2022. Multi-scenario extreme weather simulator application to heat waves. Proceedings of the Building Performance Analysis Conference and SimBuild Co-Organized by ASHRAE and IBPSA-USA, Chicago, IL, September 14–16, 49–58. doi: 10.26868/25746308.2022.C006.

Villa, D. L., and J. E. Quiroz. 2023. Reducing microgrid availability to reduce costs for coastal Puerto Rican communities. *Science and Technology for the Built Environment* 29 (9):871–86. doi: 10.1080/23744731.2023.2253087.

Villa, D. L., T. Schostek, K. Govertsen, and M. Macmillan. 2023. A stochastic model of future extreme temperature events for infrastructure analysis. *Environmental Modelling & Software* 163:105663. doi: 10.1016/j.envsoft.2023.105663.

WeatherSpark. 2023. Climate and average weather year round in Hau'ula Hawaii. Accessed September 5, 2023. https://weatherspark.com/y/137/Average-Weather-in-Hau%E2%80%98ula-Hawaii-United-States-Year-Round.

White, R. H., S. Anderson, J. F. Booth, G. Braich, C. Draeger, C. Fei, C. D. G. Harley, S. B. Henderson, M. Jakob, C.-A. Lau, et al. 2023. The unprecedented Pacific Northwest heatwave of June 2021. *Nature Communications* 14 (1):727. doi: 10.1038/s41467-023-36289-3.

Wilcox, S., and W. Marion. 2008, April. User's manual for TMY3 data sets. National Renewable Laboratories, Boulder, CO. Technical Report NREL/TP581-43156. https://www.nrel.gov/docs/fy08osti/43156.pdf.

WWA. 2023. Extreme heat in North America, Europe and China in July 2023 made much more likely by climate change. World Weather Attribution Article July 25, 2023. Accessed July 31, 2023. https://www.worldweatherattribution.org/extreme-heat-in-

north-america-europe-and-china-in-july-2023-made-much-more-likely-by-climate-change/.

Yang, Y., K. Javanroodi, and V. M. Nik. 2021. Climate change and energy performance of European residential building stocks—A comprehensive impact assessment using climate big data from the coordinated regional climate downscaling experiment. *Applied Energy* 298:117246. doi: 10.1016/j.apenergy.2021.117246.

Yassaghi, H., N. Mostafavi, and S. Hoque. 2019. Evaluation of current and future hourly weather data intended for building designs: A Philadelphia case study. *Energy and Buildings* 199:491–511. doi: 10.1016/j.apenergy.2020.115655. doi: 10.1016/j.enbuild.2019.07.016

Yassaghi, H., P. L. Gurian, and S. Hoque. 2020. Propagating downscaled future weather file uncertainties into building energy use. *Applied Energy* 278:115655. doi: 10.1016/j.apenergy.2020.115655

Zeng, Z., R. Muehleisen, J. Kim, J. New, B. Bass, P. Rastogi, J. Wang, Y. Hu, and D. Villa. 2023. A critical anlaysis of future weather data for building and energy modeling. In Pres. https://www.researchgate.net/profile/Haochen-Tan-3/publication/372411307_A_critical_analysis_of_future_weather_data_for_building_and_energy_modeling/links/64b56de38de7ed28baa48cd8/A-critical-analysis-of-future-weather-data-for-building-and-energy-modeling.pdf?origin=publication_detail.

Zhang, C., O. B. Kazanci, S. Attia, R. Levinson, and S. H. Lee. 2023. IEA EBC Annex 80—Dynamic simulation guideline for the performance testing of resilient cooling strategies: Version 2. Technical Report, DCE Technical Reports No. 306. https://backend.orbit.dtu.dk/ws/portalfiles/portal/267004362/Dynamic_simulation_guideline_DCE_report_No.299.pdf.

Zhang, C., O. B. Kazanci, R. Levinson, P. Heiselberg, B. W. Olesen, G. Chiesa, B. Sodagar, Z. Ai, S. Selkowitz, M. Zinzi, et al. 2021. Resilient cooling strategies—A critical review and qualitative assessment. *Energy and Buildings* 251:111312. doi: 10.1016/j.enbuild.2021.111312.

Zhuang, C., R. Choudhary, and A. Mavrogianni. 2023. Uncertainty-based optimal energy retrofit methodology for building heat electrification with enhanced energy flexibility and climate adaptability. *Applied Energy* 341:121111. doi: 10.1016/j.apenergy.2023.121111.